https://doi.org/10.5194/egusphere-2025-6412
Preprint. Discussion started: 26 February 2026

Lifetimes and transport characteristics of different-sized aerosols in the Asian Tropopause Aerosol Layer: a climate model study

Yuxin Dong[1236], Wenshou Tian[2], Yuan Luo[1236], Jiali Luo[2], Rui Huang[24], Haiyang Xue[25], Yifeng Peng[2]

[1]Hunan Key Laboratory of Meteorological Disaster Prevention and Reduction, Changsha, 410118, China
[2]College of Atmospheric Sciences, Lanzhou University, Lanzhou, 730000, China
[3]Hunan Meteorological Observatory, Changsha, 410118, China
[4]Tianjin Marine Central Meteorological Observatory, Tianjin Key Laboratory of Marine Meteorology, Tianjin, 300073, China
[5]School of Atmospheric Sciences, Sun Yat-sen University, Zhuhai, 519082, China
[6]Dongting Lake National Climatic Observatory, China Meteorological Administration, Yueyang, 414000, China

Correspondence to: Wenshou Tian (wstian@lzu.edu.cn)

Abstract. Using the Community Earth System Model (CESM), a series of sensitivity experiments were conducted to investigate the lifetimes and transport characteristics of different-sized aerosol particles within the Asian tropopause aerosol layer (ATAL). The results reveal that during the Asian summer monsoon (ASM) period, small particles, represented by Aitken-mode sea salt (NCl a2, 0.015–0.052 μm in diameter), can reside stably in the upper troposphere–lower stratosphere (UTLS) region and undergo extensive horizontal transport. The mean lifetime of NCl a2 particles reaches up to 552 days, while those of fine (0.095–0.56 μm) and coarse (0.63–3.70 μm) sea salt particles have an average lifetime of approximately 28 days and 11 days, respectively. The trapping effect of the ASM circulation on particles released at various heights within the ATAL (180-80 hPa) can maintain even after 120 days. When aerosol particles are released below the ATAL, the number of particles entering the UTLS region varies significantly with the release sites, i.e., aerosols released over South Asia (an effective upward transport pathway) more readily enter the ASM anticyclone and the stratosphere and reside longer in the UTLS region than particles released at the ASM anticyclone hinterland and the East Asia (EA) site.

1 Introduction

The Asian tropopause aerosol layer (ATAL) is a persistent layer of aerosols located at altitudes of 13-18 km above the Qinghai-Tibet Plateau and Iranian Plateau during the Asian summer monsoon (ASM) period, spanning from June to September (Vernier et al., 2011). Since its discovery from observations using the CALIPSO satellite, the existence of the ATAL has been confirmed by multi-source observations, including satellite observations, aircraft sounding, and ground-based observations (Thomason and Vernier, 2013; Appel et al., 2022; Mahnke et al., 2021). Previous studies reported that the aerosol particles within the ATAL originate mainly from anthropogenic emissions in South and East Asia (Yu et al., 2015; Fairlie et al., 2020; Clemens et al., 2024). These particles are transported upward to the upper troposphere–lower

https://doi.org/10.5194/egusphere-2025-6412
Preprint. Discussion started: 26 February 2026

stratosphere (UTLS) region through preferred pathways over the Himalayas-Gangetic Plain and the Sichuan Basin (Lau et al., 2018; Yuan et al., 2019). Furthermore, data from CALIPSO and the StratoClim project have confirmed the critical role of deep convection over the Tibetan Plateau in the formation of the ATAL (Vernier et al., 2015; Appel et al., 2022). Numerical modeling studies, including climate models, chemical transport models, and Lagrangian transport models, have further revealed key transport mechanisms of ATAL aerosols. These studies show that the spiral upward motion along isentropic surfaces from the upper troposphere to the lower stratosphere within the ASM anticyclone can lift aerosol particles—initially transported by deep convection to the upper troposphere—further into the ATAL (Yu et al., 2017; Ma et al., 2019; Zhang et al., 2020). Thus, the formation of the ATAL is closely linked to the ASM circulation, particularly the ASM anticyclone and deep convective activity.

During the ASM period, the average mass concentration of aerosols inside the ATAL remains relatively stable, indicating a rough balance between sources and sinks (Yuan et al., 2019). However, previous studies have primarily focused on the sources of ATAL particles, while their sinks and residence characteristics in the UTLS region are not yet fully quantified. The vertical and horizontal distribution of aerosol particles inside and outside the ASM region determines whether they can be transported and dispersed more widely via large-scale circulation (e.g., the Brewer–Dobson circulation). This large scale transport, in turn, allows the particles to exert broader climate effects (Garny and Randel, 2016). Limited by the scarcity of sounding observations, systematic investigation of the transport characteristics of aerosols within the ATAL during and after the monsoon period, as well as their climate effects, remains challenging (Tian et al., 2023). To quantitatively evaluate the residence time of ATAL aerosols in the UTLS region and the influence of the ASM circulation on their distribution, this study employs two key metrics: aerosol lifetime and the duration of confinement by the ASM anticyclone.

The aerosol particles within the ATAL affect the local radiation balance through direct and indirect climate effects (Mohanakumar, 2008; Cziczo et al., 2019; Gao et al., 2023). They also impact on stratospheric ozone distribution via two key pathways: radiation-dynamics-chemistry feedback (Rosenlof, 2018; Solomon, 2023; Tian et al., 2025) and the stratosphere-troposphere exchange (Su et al., 2011). These processes together modulate the thermal and dynamical structure of the UTLS region.

Previous studies have made preliminary estimates of the radiative effects of ATAL. However, most of these studies have relied on simplified radiative transfer models (Vernier et al., 2015; Gao et al., 2023). It is noteworthy that particle size and the lifetime of particles in the atmosphere are crucial factors influencing the total radiative effect of aerosols (Murphy et al., 2021). Therefore, systematically investigating the transport characteristics and atmospheric lifetimes of particles of different sizes in the UTLS region is essential for accurately assessing the overall climate effects of ATAL.

Accordingly, this study designs a series of idealized experiments using the Community Earth System Model (CESM) to investigate the differences in transport characteristics and lifetimes of aerosol particles with different sizes in the UTLS region, as well as the main factors impacting on the lifetimes of ATAL particles. The paper is structured as follows: Sect. 2 introduces the CESM model and the methodology for calculating key quantities such as aerosol lifetime and the duration of

https://doi.org/10.5194/egusphere-2025-6412
Preprint. Discussion started: 26 February 2026

confinement by the ASM anticyclone; Sect. 3 presents the main results from the series of idealized numerical experiments; Sect. 4 gives the main conclusion and some remarks.

2 Data, model and methods

2.1 MERRA-2 reanalysis data

MERRA-2 (The Modern-Era Retrospective Analysis for Research and Applications, Version 2) reanalysis dataset is developed by NASA's Global Modeling and Assimilation Office and represents the latest generation of reanalysis datasets that incorporate modern satellite observations (Gelaro et al., 2017). This dataset covers a wide range of variables, including atmospheric radiation, chemistry, physics, and meteorological fields, with global coverage at a horizontal resolution of 1.5°×1.5°. This study uses monthly horizontal wind fields, geopotential height fields, and temperature data in pressure coordinates for the year 2000.

2.2 Aerosol lifetime

Aerosol lifetime is determined by the efficiency of removal processes—such as dry deposition and wet scavenging (Rasch et al., 2000; Textor et al., 2006), and served as an indicator of the potential for long-range transport of atmospheric components (Kaneyasu et al., 2012). This metric is widely used to quantify the residence time of atmospheric components in the entire atmosphere or specific regions, and a longer lifetime indicates a greater potential for climate effects. Previous studies have used this metric to estimate lifetimes of pollutants from surface emissions (Croft et al., 2014; Kristiansen et al., 2016), volcanic aerosols (Beirle et al., 2014; Li and Cohen, 2021), and greenhouse gases (Li et al., 2022).

This study uses the 2-month mean aerosol lifetime ($\tau_{2\ mo}$) from a two-month time series of aerosol mass concentration, defined as follows:

$$\tau_{2\ mo} = \frac{\sum_{t=0}^{t=2\ mo} C(t)}{\sum_{t=0}^{t=2\ mo} D(t)}, \quad (1)$$

where *C(t)* is the global aerosol mass burden at time t, and *D(t)* denotes the aerosol mass loss rate during a timestep Δt, representing the total mass removed by deposition processes during that interval. In the case of a pulse emission, the mean aerosol lifetime over a longer time scale approximates the steady-state aerosol lifetime, and its value is primarily controlled by intense scavenging during the initial days after emission. Thus, a longer mean aerosol lifetime indicates weaker short-term removal intensity (Croft et al., 2014).

2.3 The CESM-MAM7 model

Global-scale simulations are conducted using the CESM 1.2.2 developed by the National Center for Atmospheric Research (NCAR). CESM is a fully coupled global climate model, the atmosphere dynamic module used in this paper is the Community Atmosphere Model (CAM5.3), coupled with the Modal Aerosol Model (MAM7) to simulate aerosol and

https://doi.org/10.5194/egusphere-2025-6412
Preprint. Discussion started: 26 February 2026

chemistry processes. This configuration has been verified in previous studies as capable of accurately simulating ATAL-related physical and chemical properties (Bossolasco et al., 2021).

The MAM7 module simulates the transport of 31 aerosol tracers and 6 gas species. It numerically represents aerosol internal and external mixing, nucleation, coagulation, condensation, dry deposition, wet removal, and chemical transformation of aerosol precursors (Liu et al., 2012). Aerosols in MAM7 are categorized into seven modes: accumulation mode (a1, 0.056–0.26 μm), Aitken mode (a2, 0.015–0.052 μm), primary carbon (a3, 0.039–0.13 μm), fine sea salt (a4, 0.095–0.56 μm), fine soil dust (a5, 0.14–0.62 μm), coarse sea salt (a6, 0.63–3.70 μm), and coarse soil dust (a7, 0.59–2.75 μm). The specific size distribution for each mode follows a log-normal assumption (Easter et al., 2004; Liu et al., 2012).

Modal transfer occurs only among the Aitken, primary carbon, and accumulation modes via coagulation and condensation processes (Easter et al., 2004; Liu et al., 2012). The H_2SO_4–NH_3–H_2O ternary parameterization scheme (Merikanto et al., 2007) and boundary layer nucleation parameterizations (Sihto et al., 2006; Wang et al., 2009) enable MAM7 to simulate new particle formation in the Aitken mode. Through aqueous chemistry and condensation, Aitken mode particles can grow into the size range typical of the accumulation mode. Coagulation processes within and between the Aitken, accumulation, and primary carbon modes further facilitate mass transfer from the Aitken and primary carbon modes into the accumulation mode (Binkowski and Roselle, 2003; Easter et al., 2004).

2.4 Model evaluation and numerical experiments

The control experiment runs from 1 January 1998 to 31 December 2001, with the first year discarded as spin-up. The model's default initial fields are used to initialize the simulation. The horizontal resolution is 1.9°×2.5°, with 30 vertical layers (including 11 layers within the 400–70 hPa range), and a model top near 3 hPa. In the control experiment, interactive coupling exists among the atmospheric (CAM5.3), land (CLM4), and river runoff (RTM) modules, while the sea ice module (CICE) uses preprocessed data.

The chemical emissions used in the experiments are the model's default emission sources, which integrate data from multiple inventories, including POET, the Regional Emission inventory in ASia (REAS), the Global Fire Emissions Database (GFED2), the Intergovernmental Panel on Climate Change (IPCC), and AeroCom. These encompass natural (e.g., volcanic and marine), anthropogenic (e.g., transportation, industrial, agricultural, and waste management), and biomass burning emissions. All surface and external emission sources are fixed at their global year 2000 levels.

To evaluate the model's performance in simulating the ASM circulation, Fig. 1 presents a comparison between the simulated meteorological fields and MERRA-2 reanalysis data for summer 2000 (corresponding to the emission state) regarding temperature, geopotential height, and horizontal wind in the UTLS region. The results show that the model well reproduces the horizontal distribution of geopotential height, the spatial extent of the ASM anticyclone, as well as the vertical temperature structure. Since the temperature and geopotential height characterize key features of the tropopause and the ASM anticyclone (Mohanakumar, 2008; Bian et al., 2009), Fig. 1 indicates that the model is able to reliably capture the ASM circulation characteristics in the UTLS region.

https://doi.org/10.5194/egusphere-2025-6412
Preprint. Discussion started: 26 February 2026

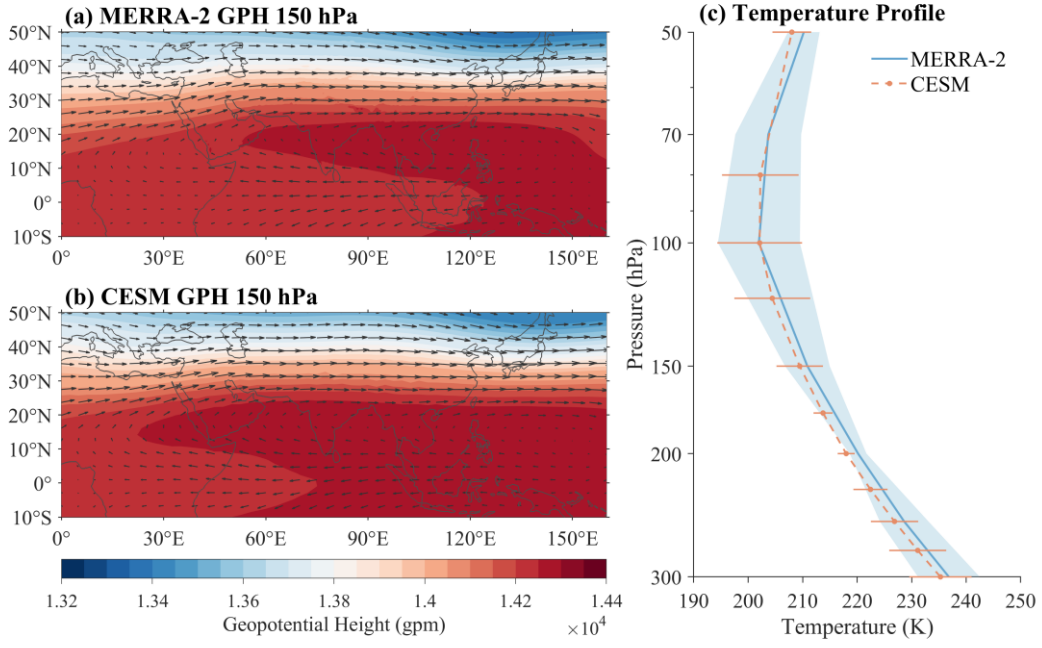

Figure 1: The latitude-longitude cross-sections of geopotential height and horizontal wind at 150 hPa averaged in 2000 which are derived from (a) MERRA-2 reanalysis dataset, (b) the model simulation and (c) vertical profile of ATAL-averaged (15−45° N, 0−160° E) temperature, where blue solid line represents MERRA-2 data, orange dashed line presents simulation result, shadows and horizontal error bars present the standard deviation of the data (units: gpm, K).

To estimate the transport characteristics of different-sized aerosol particles in the ATAL and the stratosphere, sea salt (NCl) aerosols are used as target species. These particles are chosen as they do not engage in any chemical reactions (treated as passive tracers), and exert minimal radiative effects. To ensure differentiation among the particle size ranges of the released particles, specific aerosol modes are selected based on the typical size distributions of MAM7 aerosol modes. The target modes include the Aitken mode (a2, 0.015–0.052 μm), which represents smaller particle sizes, fine sea salt (a4, 0.095–0.56 μm), and coarse sea salt (a6, 0.63–3.70 μm), representing larger particle sizes. As mentioned in Sect. 2.3, NCl a2 particles experience continuous growth through liquid-phase chemical processes or coagulation processes after release, until they reach the size range of a1 particles. This growth signifies mass transfer process from a2 particles to a1 particles, which is not observed in a4 and a6 particles (Binkowski and Roselle, 2003; Easter et al., 2004). Therefore, in the analysis of experimental results, NCl a2 particles correspond to a mixture of a2 particles and the transformed a1 particles.

The idealized numerical experiments share the same model configuration as the control experiment. A total mass of 0.5 Tg of NCl particles (approximately equivalent to the aerosol emissions from a moderate volcanic eruption) is released between 12–18 UTC on 8 June 2000 (a date selected based on climatological mean dynamic fields). The experiments differ in the combinations of particle size (a2, a4, and a6), release location, and release altitude. As shown in Fig. 2, three particle release areas are chosen in consideration of the high polluted areas, including South Asia (SA, 75–85° E, 20–30° N), East Asia (EA, 110–120° E, 25–35° N), and the climatological mean ASM anticyclone hinterland (65–75° E, 25–35° N) (Fairlie et al., 2020;

https://doi.org/10.5194/egusphere-2025-6412
Preprint. Discussion started: 26 February 2026

Shaddick et al., 2020). The release height is selected by considering the average summer tropopause height of the focused region and the vertical range of ATAL, which spans from 13 to 18 km above the sea level (Johnston and Xie, 2020; Vernier et al., 2011): 11–12 km (middle-upper troposphere, below the ATAL), 14–15 km (upper troposphere, within the ATAL), and 16–17 km (lower stratosphere, within the ATAL). This selection enables a multidimensional assessment of aerosol transport characteristics at different altitudes.

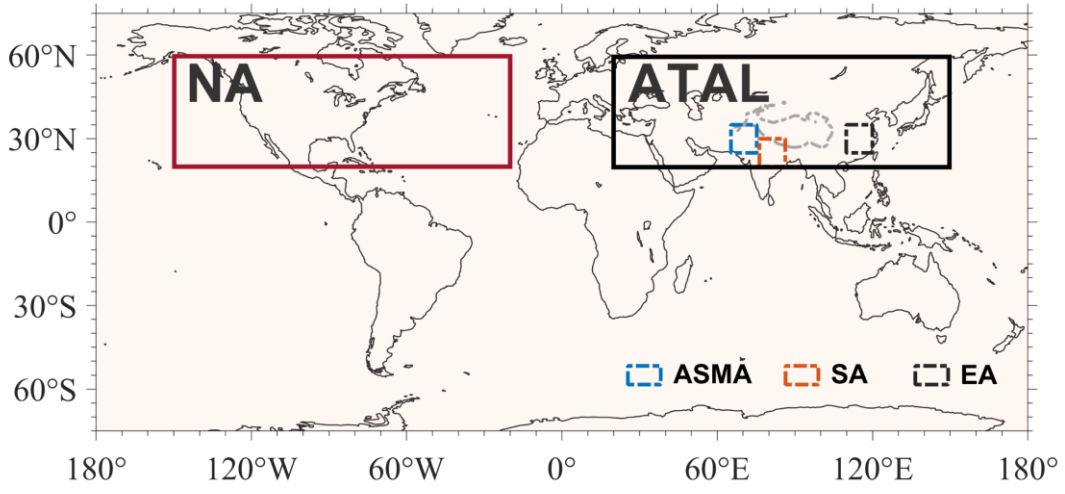

Figure 2: Schematic diagram of the North American (NA) region, ATAL region and particle release area, the solid boxes in dark red and black represent the NA region and the ATAL region, the dashed boxes in blue, orange and black represent the Asian Sumeer Monsoon (ASM) anticyclone hinterland release site, the South Aisa (SA) release site and the East Asia (EA) release site, with the outline of the Tibetan Plateau marked by gray dotted line.

To quantify the impact of the ASM anticyclone on aerosol transport characteristics in the ATAL region, we compare the North American region (NA, 20−60° N, 20−150° W) with the ATAL region (20−60° N, 20−150° E), both located at the same latitude and having the same horizontal extent (regional boundaries are shown in Fig. 2). Furthermore, based on temporal variations of the average aerosol mass concentration in the NA and ATAL regions, we define the ASM anticyclone confinement duration as the number of days during which there is a significant difference in the average aerosol mass concentration between the ATAL and NA regions at the 99% significance level. The significance test is conducted using a two-sided Student's t-test. We select the average mass concentration time series of aerosol for a 9-day period, including the t-th day and 4 days before and after, as the test sequence (referencing the sliding T-test). The confinement duration is defined as the earliest time t (in days) at which the difference between the two regions first fails the significance test.

To ensure comparability across experiments, the direct radiative effect of NCl aerosols was disabled. A total of 27 independent experiments were conducted, each with a distinct combination of particle size, release location, and release height.

https://doi.org/10.5194/egusphere-2025-6412
Preprint. Discussion started: 26 February 2026

3 Model results

Fig. 3 shows the temporal evolution of the averaged mass concentration within the ATAL region (15–45° N, 0–160° E) for NCl a2 (small-size), a4 (medium-size), and a6 (large-size) particles released at 16–17 km. The results indicate that particle size governs the residence characteristics within the UTLS region. After release, Aitken-mode NCl a2 particles can reside stably inside the stratosphere with a very slow removal rate. Even after 115 days (by 30 September), the regional mean mass concentration remains above 1/20th of its peak value. Medium-sized NCl a4 particles are removed more rapidly, with the regional mean mass concentration dropping below 1/20th of the peak value approximately 30 days after release. The largest NCl a6 particles, for which gravitational deposition dominates over buoyancy, exhibit very rapid gravitational sedimentation and sink completely below the mid-troposphere (400 hPa) within a few days after release.

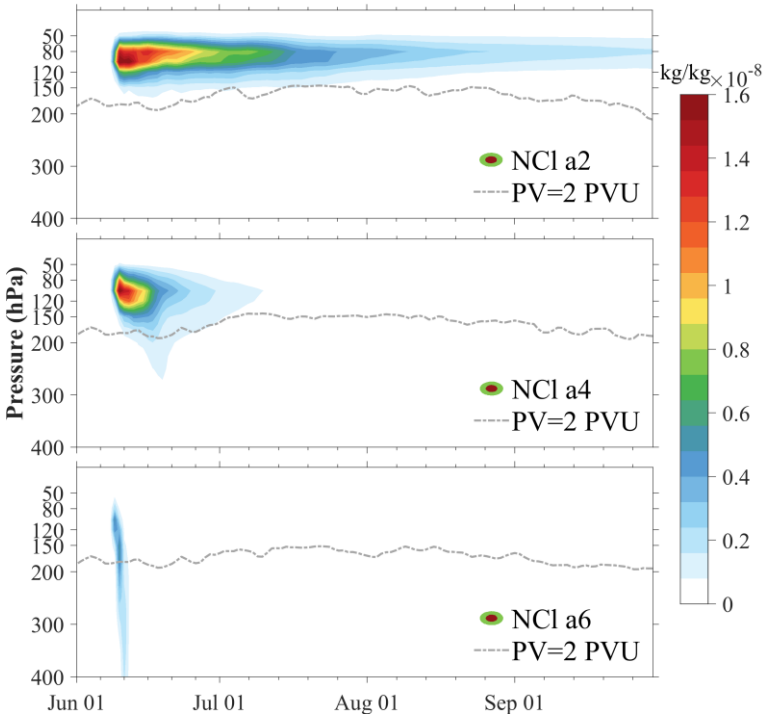

Figure 3: Time series of the averaged mass concentration for NCl a2 (top), a4 (middle), and a6 (bottom) particles released at 16–17 km within the ATAL region. The gray dot-dashed line indicates the regional mean tropopause height (units: kg/kg).

To further explore the residence time of particles of different sizes in the stratosphere, Fig. 4 presents the time series of mass concentration for NCl a2 and a4 particles released at various altitudes and release sites. We can note that the average mass concentration of the smallest NCl a2 particles in the stratosphere increases rapidly within days after release, followed by a brief decline and then a slow increase over the subsequent 30 days. This evolution is typical of tracer transport from the upper troposphere into the stratosphere (Chen et al., 2022; Tian et al., 2023). NCl a2 particles can reside stably within the stratosphere until the end of the ASM period (May–September); thereafter, their stratospheric mass concentration begins to decline gradually. NCl a4 particles also exhibit concentration fluctuations within the first ~30 days. However, owing to their

https://doi.org/10.5194/egusphere-2025-6412
Preprint. Discussion started: 26 February 2026

larger mass and continuous dry deposition, they gradually leave the UTLS region, and their average mass concentration decreases steadily.

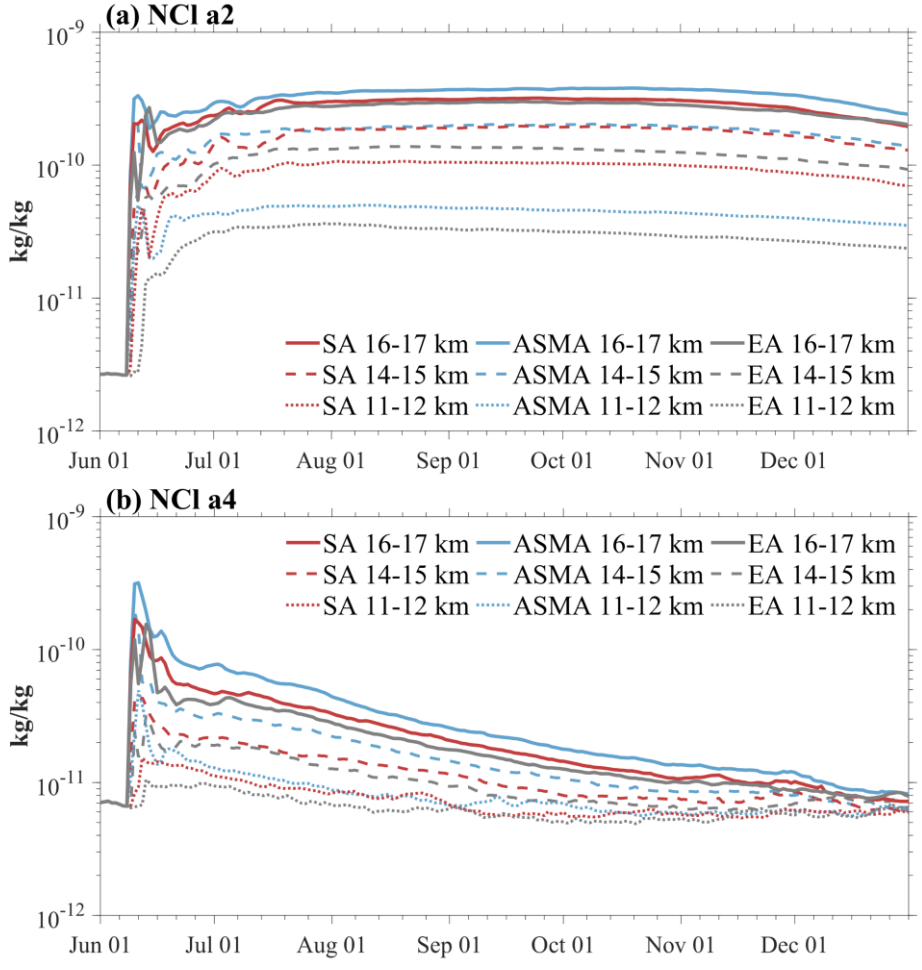

Figure 4: The simulated time series of the average stratospheric mass concentration of (a) NCl a2 and (b) a4 particles released at different locations (red for SA, blue for ASM anticyclone hinterland, gray for EA). Line styles denote release altitude: thick solid line for 16–17 km, dashed line for 14–15 km, and chain-dotted line for 11–12 km (unit: kg/kg).

By comparing experiments with the same particle size and release location but different release altitudes, we find that the mass of NCl particles able to cross the tropopause into the stratosphere increases with release heights. Further comparison of experiments in which particles are released at different sites reveals that for particles released inside the ATAL (at 14–15 km and 16–17 km), the average stratospheric mass concentration of particles released at the ASM anticyclone hinterland is the largest, and the average stratospheric mass concentration of particles released at East Asia is the smallest. This result is consistent with the previous findings that the ASM anticyclone is dominate factor impacting on the stratosphere-troposphere mass exchange (STE) in the UTLS region during the ASM period. The closed streamlines around the ASM anticyclone have a trapping effect, which causes the atmospheric components to reside within the ASM anticyclone for a relatively long time,

https://doi.org/10.5194/egusphere-2025-6412
Preprint. Discussion started: 26 February 2026

and to be isolated and unable to exchange with the air outside the anticyclone (Bian et al., 2020; Wu et al., 2023). Consequently, the combined effect of this trapping effect and the widespread spiral uplift within the anticyclonic region enables more NCl particles released in the ASM anticyclone hinterland to enter the stratosphere.

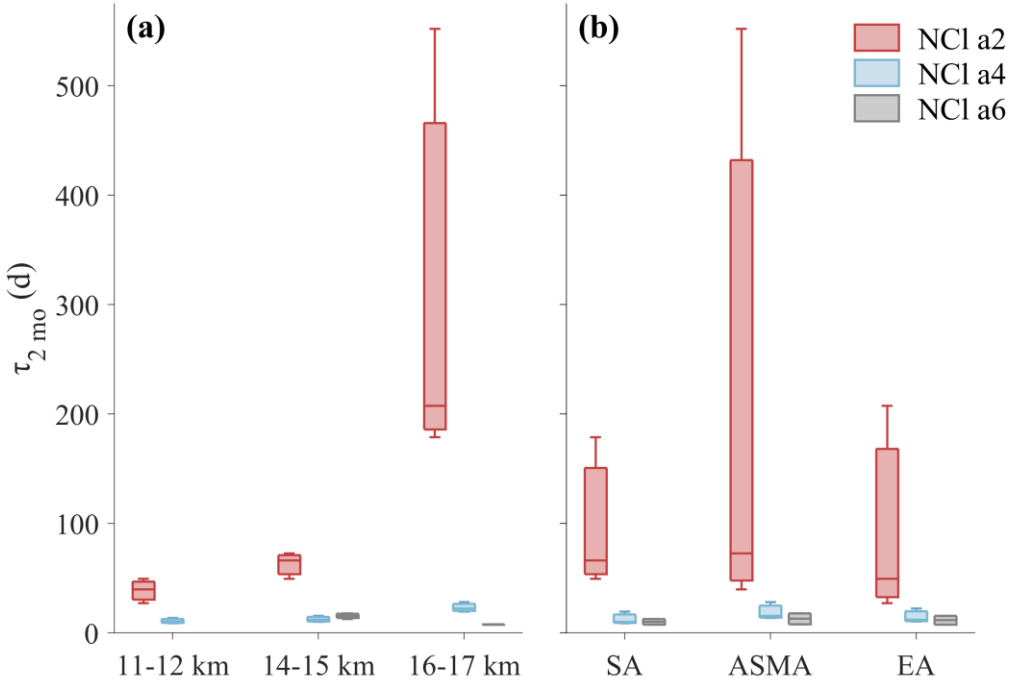

Figure 5: Box plots of $\tau_{2\ mo}$ for NCl a2 (red), NCl a4 (blue), and NCl a6 (gray) simulations in the UTLS region (200-50 hPa), (a) for different release altitudes, and (b) for different release locations. The horizontal line, bottom edge, and top edge inside the box denote the median, lower quartile, and upper quartile, respectively, while the whisker endpoints correspond to the maximum and minimum lifetimes (unit: days).

The aerosol lifetime is commonly used to quantify the residence time of aerosols in the entire atmosphere or specific regions. Fig. 5. displays grouped box plots of the two-month mean lifetime ($\tau_{2\ mo}$) of NCl a2, a4, and a6 particles released at various altitudes and release sites. As expected, the particle size has a substantial influence on the lifetime of NCl particles in the UTLS region. As mentioned earlier, the value of $\tau_{2\ mo}$ is primarily governed by the intense removal processes occurring during the first few days after release, where gravitational deposition serves as the dominant removal mechanism for aerosol particles in the UTLS region (Zhang et al., 2015). Aerosol particles of different sizes exhibit distinct deposition velocities due to differences in the relative magnitudes of gravitational and buoyancy forces: the smallest NCl a2 particles have the lowest deposition velocity, while a6 particles have the highest. Consequently, regardless of the release location, a2 particles exhibit the longest $\tau_{2\ mo}$ due to their slowest removal rate, with a maximum value reaching 552 days and a median of approximately 66 days after excluding outliers. NCl a4 particles have shorter $\tau_{2\ mo}$, with a maximum of 28 days and a median of about 14 days. Due to their extremely rapid removal, a6 particles have an average $\tau_{2\ mo}$ of only about 11 days. These

https://doi.org/10.5194/egusphere-2025-6412
Preprint. Discussion started: 26 February 2026

results are consistent with the qualitative conclusions drawn from Figs. 3 and 4, confirming that for aerosol particles within the ATAL, smaller sizes correspond to longer residence times in the UTLS region.

Further analysis of Fig. 5a reveals that the $\tau_{2\,mo}$ of NCl a2 and a4 particles increases as the particle release altitude rises. It is also notable that when the release altitude increases from below the ATAL (11–12 km) to within the ATAL (14–15 km), the $\tau_{2\,mo}$ of a2 particles shows a marginal change. However, within the ATAL, when the release altitude increases from 14–15 km (below the tropopause) to 16–17 km (within the stratosphere), the $\tau_{2\,mo}$ of a2 particles increases rapidly, exceeding three times the value at the lower altitude. This can be attributed to the stronger vertical mixing and convection present in the troposphere compared to that in the stratosphere, which significantly accelerates the removal of tropospheric particles (Ohata et al., 2016). Therefore, the particle release altitude relative to the tropopause plays a crucial role in determining the strength of the early removal process, which is reflected in the value of $\tau_{2\,mo}$.

Consistent with the results in Fig. 4, the release location also influences the lifetime of particles within the UTLS region (Fig. 5b). Comparison across different release sites shows that for both NCl a2 and a4 particles released within the ATAL (at 14–15 km and 16–17 km) over the ASM anticyclone hinterland, the $\tau_{2\,mo}$ is the longest. This feature is particularly pronounced for particles with smaller sizes, i.e., when considering NCl a2 particles released at the altitude of 16–17 km, the $\tau_{2\,mo}$ value for the ASM anticyclone hinterland release site is more than double that of the SA and EA release sites, reaching 552 days. This phenomenon can also be attributed to the stable presence of the ASM anticyclone and its associated trapping effect within the UTLS region during the monsoon season.

Following the investigation of bulk properties of particle deposition and residence, we further examine the influence of release location on the spatial distribution of particles within the UTLS region. Given that NCl a2 particles exhibit the longest lifetime and the most extensive transport scale among the three focused particle sizes, we select these particles as the primary tracer for all subsequent analyses, to further characterize aerosol transport characteristics through climate model simulations. Fig. 6 presents the vertical global probability density distributions for NCl a2 particles released at different locations within the ATAL (from day 10 to 120 after release; key time steps are selected for display due to space constraints). During the first 30 days after release, the vertical distributions of aerosol particles vary significantly with the different release locations. The altitude of the maximum probability density varies depending on the release height, with particles released at 16–17 km generally distributed at higher altitudes. In experiments with both release heights, the altitude of the maximum probability density is higher than the initial release height, this feature is potentially linked to the convective activity in the ASM region and the widespread uplift within the ASM anticyclone (Tobo et al., 2007; Yu et al., 2017; Lau et al., 2018; Ma et al., 2019; Yuan et al., 2019; Zhang et al., 2020).

It is apparent that particles released within the ATAL and inside the ASM anticyclone hinterland can be lifted to higher altitudes. Starting from day 50 after release, the differences in vertical distribution among particles from different release locations gradually diminish, and the influence of release height on their vertical distribution weakens. Also note that the altitude of the maximum probability density for NCl a2 particles gradually decreases. However, due to the trapping effect of atmospheric constituents by the ASM anticyclone (Bian et al., 2020; Wu et al., 2023), the particles remain primarily within

https://doi.org/10.5194/egusphere-2025-6412
Preprint. Discussion started: 26 February 2026

the UTLS region, with the dominant height lowering from 120–80 hPa in the early stage (days 10–60) to 180–80 hPa later (days 70–120).

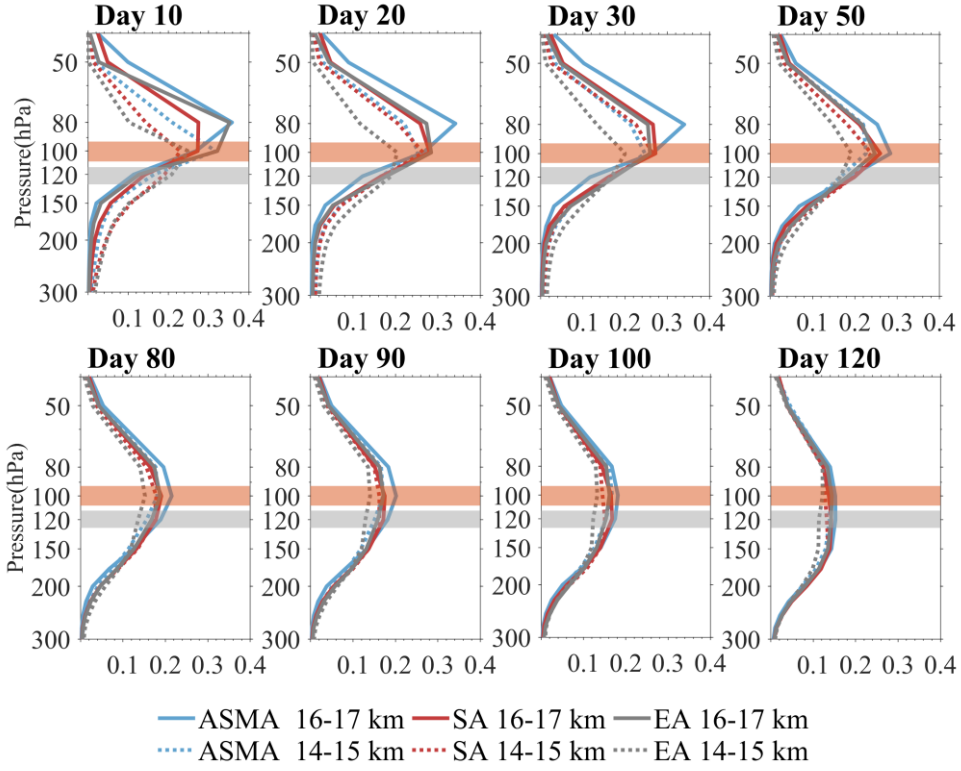

Figure 6: Mean vertical distribution of NCl a2 particles after the release at different release locations, where solid lines represent releases at 16-17 km, dashed lines denote releases at 14-15 km. The lines in blue, red, and gray denote the ASM anticyclone hinterland release site, SA release site, and EA release site, respectively. The orange (16-17 km) and gray (14-15 km) bars indicate the initial release height.

To show more details of the horizontal distribution of NCl particles in the UTLS region, Fig. 7 gives the horizontal probability density distribution of NCl a2 particles released at the ASM anticyclone hinterland and the EA release site at 14–15 km (the transport characteristics of particles released over SA release site are similar to those from the ASM anticyclone hinterland and are not shown).

Owing to the trapping effect of the ASM anticyclone on aerosol particles, during the first 40 days after release, NCl a2 particles from both release sites remain predominantly inside the anticyclone. A small fraction disperses outside the anticyclone with air detaching from its edges, and the horizontal distribution of these particles outside the ASM anticyclone gradually becomes more uniform. As dispersion continues, for particles released at the ASM anticyclone hinterland at 14–15 km, a region of high probability density persists in the Northern Hemisphere mid-latitudes even 80 days after the instantaneous aerosol release. In contrast, the horizontal distribution outside the Northern Hemisphere mid-latitudes becomes nearly uniform. The EA release site, located near the edge of the ASM anticyclone, experiences different atmospheric circulation conditions compared to the ASM anticyclone hinterland and SA sites. Aerosol particles released at this site

https://doi.org/10.5194/egusphere-2025-6412
Preprint. Discussion started: 26 February 2026

disperse more extensively and rapidly outside the anticyclone, and a greater number reach the UTLS region of the Southern Hemisphere. Eighty days after the instantaneous NCl a2 particle release over EA site, bands of high distribution probability density are present in the mid-latitudes of both the Southern and Northern Hemispheres.

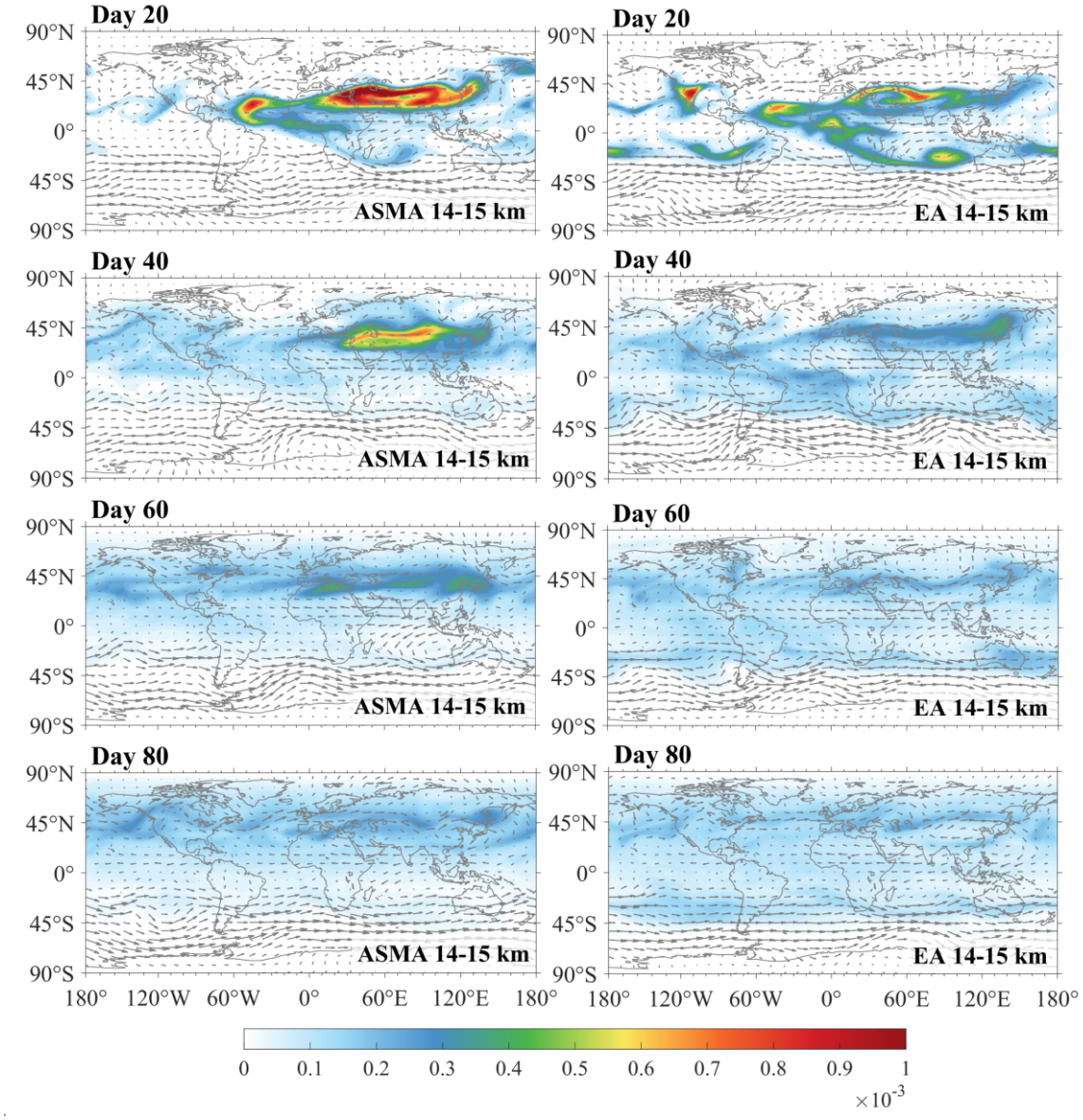

Figure 7: Mean probability distribution functions of NCl a2 particles released at the ASM anticyclone hinterland (left) and EA (right) release site at 14-15 km, overlaid with horizontal wind vectors (gray arrows).

Analysis of Figs. 4–7 indicates that the transport characteristics and atmospheric lifetime of aerosols within the ATAL are primarily influenced by the ASM circulation, with the ASM anticyclone being one of the dominant weather systems. To quantitatively analyze the trapping effect of the ASM anticyclone on aerosol particles released at different locations, Fig. 8

https://doi.org/10.5194/egusphere-2025-6412
Preprint. Discussion started: 26 February 2026

presents the time series of the average mass concentration of NCl a2 particles in the UTLS region (200–50 hPa) for both the ATAL and NA regions (see Fig. 2). The subplots show the ratio of the total mass of NCl a2 particles in the ATAL region to the total mass in the Northern Hemisphere for particles released at different release sites; this ratio reflects the relative number of particles that enter the ASM anticyclone center.

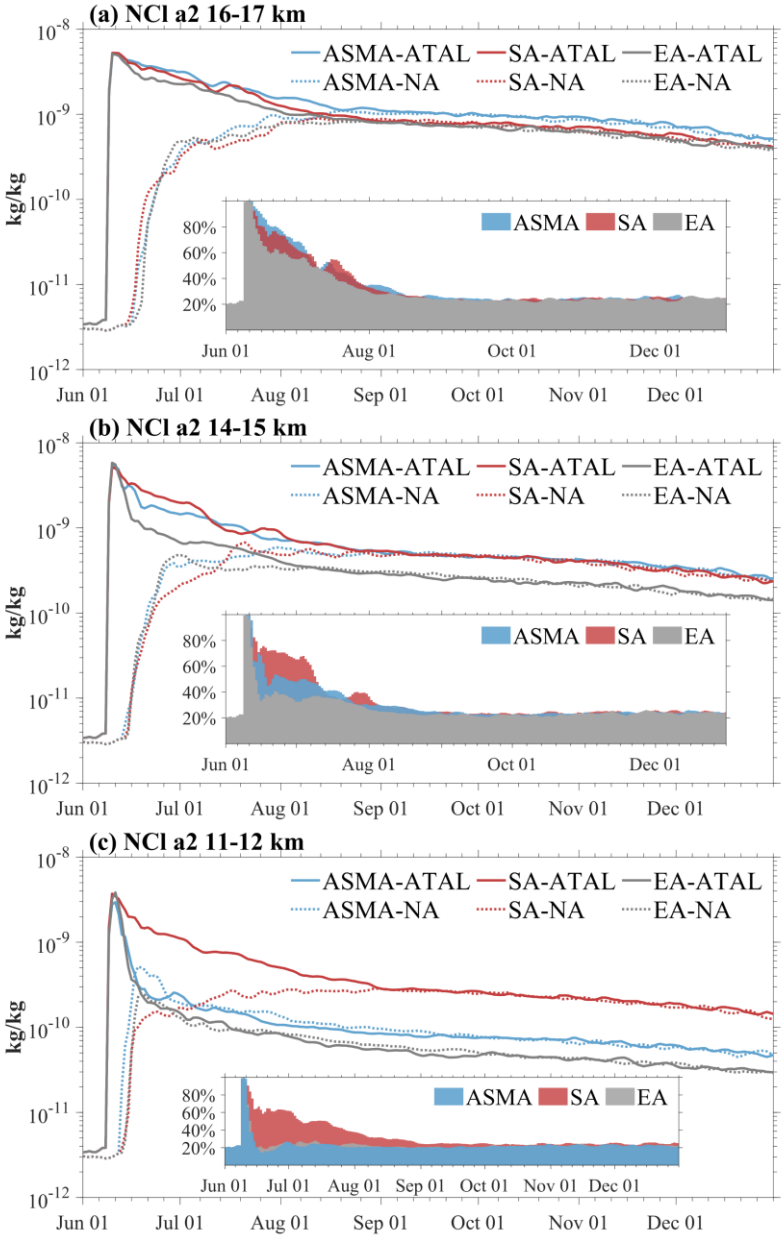

Figure 8: Time series of the average mass concentration of NCl a2 particles within the 200–50 hPa height range, after release at (a) 16–17 km, (b) 14–15 km, and (c) 11–12 km, for the ATAL region (solid lines) and the NA region (dashed lines). Blue lines denote release at the ASM anticyclone hinterland, red lines the SA site, and gray lines the EA site. Subplots show the ratio of the total NCl a2 particle mass in the ATAL region to the total mass in the Northern Hemisphere after release (units: kg/kg).

https://doi.org/10.5194/egusphere-2025-6412
Preprint. Discussion started: 26 February 2026

Due to horizontal transport, the mass concentration of a2 particles in the NA region increases rapidly approximately 10 days after release, with this rapid increase lasting about 10 days. Meanwhile, the average mass concentration in the ATAL region continuously decreases and gradually converges with that in the NA region (in experiments with releases at 14–15 km and 16–17 km, the average mass concentration in the NA region undergoes a period of slow increase). This indicates that over simulation time, the horizontal distribution of aerosol particles in the Northern Hemisphere UTLS region becomes more uniform, implying that the influence of the ASM anticyclone on particle distribution gradually diminishes. Accordingly, we define the ASM anticyclone confinement duration as the number of days after release during which a statistically significant difference (at the 99% confidence level) exists between the average aerosol mass concentrations in the ATAL and NA regions (details in Sect. 2.4). The calculated confinement durations for each numerical experiment are listed in Table 1.

Table 1: The duration of anticyclonic confinement calculated from the time series of the average mass concentration of NCl a2 and NCl a4 particles within the 200−50 hPa range for the ATAL and NA regions. (unit: day).

Release sites	Release height	Duration of anticyclonic confinement (day)	
		NCl a2	NCl a4
ASMA	16−17 km	109	86
	14−15 km	91	73
	11−12 km	15	14
SA	16−17 km	86	68
	14−15 km	99	61
	11−12 km	92	20
EA	16−17 km	86	64
	14−15 km	70	34
	11−12 km	15	14

Combining Fig. 8 and Table 1, the confinement duration of NCl a2 particles by the ASM anticyclone varies significantly with the release altitude, i.e., the higher release altitude corresponds to a stronger trapping effect. For NCl a2 particles released at 16–17 km and 14–15 km, the average confinement duration is approximately 93.7 days and 86.7 days, respectively. When the particles are released below the ATAL region (11–12 km), the confinement duration is only about 40.7 days.

Furthermore, NCl a2 particles released at different locations exhibit different confinement durations. For releases at 16–17 km, the confinement duration is longest for the ASM anticyclone hinterland release site, while the durations for the SA and EA sites are essentially similar. Within about 60 days after release, the proportion of particles entering the anticyclone center is largest when particles are released at ASM anticyclone hinterland and smallest when particles are released at EA. After 60

https://doi.org/10.5194/egusphere-2025-6412
Preprint. Discussion started: 26 February 2026

days, the proportions across experiments become generally consistent. This suggests that NCl a2 particles released at 16–17 km from different locations achieve a similar horizontal distribution after approximately 60 days.

The results for particles released at 14–15 km and 11–12 km differ from those at 16–17 km. The proportion of NCl a2 particles entering the ASM anticyclone center is largest when particles are released at SA and smallest when particles are released at EA. When the release height is lowered to 11–12 km (below the ATAL), the mass proportion of particles in the ATAL region relative to the total Northern Hemisphere drops to the pre-release level within 10 days for both the ASM anticyclone hinterland and EA site. The confinement duration for NCl a2 particles at these two sites also decreases markedly to 15 days. In the SA release site experiment, the high value of the mass proportion in the ATAL region relative to the Northern Hemisphere total is maintained for a longer time, significantly differing from the other sites. This indicates that a greater proportion of NCl a2 particles in this experiment are transported upward into the anticyclone center compared to the others, allowing them to reside longer within the ATAL region and experience a longer trapping effect by the ASM anticyclone, up to 70 days. This result is consistent with Fig. 4, demonstrating that during the ASM period, the region over SA (the Indian subcontinent) serves as an effective pathway for transporting aerosol particles from lower altitudes to the upper troposphere and even into the stratosphere.

4 Conclusions and Discussion

Atmospheric aerosol lifetime is one of the most crucial factors in estimating aerosols' climate effects. However, the lifetimes of different-sized aerosols in the UTLS region have not been well quantified in the previous studies due to shortage of in situ measurements. Using the CESM model, the lifetimes of different-sized aerosols and the duration of the ASM anticyclone confinement of aerosols are diagnosed in this study. The numerical experiments demonstrate that during the ASM period, small particles, represented by Aitken-mode sea salt (NCl a2, 0.015–0.052 μm), can reside stably within the stratosphere. Their two-month mean lifetime ($\tau_{2\ mo}$) reaches up to 552 days, with a median of approximately 66 days after excluding outliers. These particles also undergo extensive horizontal transport. Larger NCl a4 particles (0.095–0.56 μm) leave the UTLS region more quickly and exhibit a smaller horizontal transport range compared to NCl a2 particles, with a maximum $\tau_{2\ mo}$ of 28 days and a median of about 14 days. The largest NCl a6 particles (0.63–3.70 μm) are subject to gravitational deposition, which dominates over buoyancy. They therefore deposit rapidly via gravitational sedimentation, resulting in an average $\tau_{2\ mo}$ of only about 11 days.

As the ASM anticyclone confines most aerosol particles within the ATAL, the vertical deposition process of particles inside the anticyclone is relatively slow. NCl a2 particles released inside the ATAL remain primarily within the 120–80 hPa range for up to 60 days. Even after 120 days, the main vertical distribution of NCl a2 particles descends only to the 180–80 hPa altitudes, still predominantly within the UTLS region. Regarding the horizontal transport characteristics of small NCl a2 particles, they exhibit minimal diffusion outside the ASM anticyclone during the first 20 days after release, with the majority remaining inside the anticyclone for the first 40 days. By 80 days after release, the region of high probability density within

https://doi.org/10.5194/egusphere-2025-6412
Preprint. Discussion started: 26 February 2026

the Northern Hemisphere mid-latitudes gradually dissipates, and the horizontal distribution becomes nearly uniform across the UTLS region between 20° S and 60° N.

The atmospheric circulation near the aerosol release location also influences particle transport in the UTLS region. When aerosols are released inside the ATAL (at 14–15 km and 16–17 km), the trapping effect of the ASM anticyclone varies with the release site's relative position to the anticyclone center. This leads to differences in aerosol distribution, transport characteristics, and aerosol lifetimes among experiments. The average stratospheric mass concentration of NCl a2 and a4 particles, their $\tau_{2\ mo}$ in the UTLS region, and the ASM anticyclone confinement duration are all greater for the ASM anticyclone hinterland and South Asian (SA) release sites compared to the East Asian (EA) site. However, NCl a2 particles released at the EA site (on the edge of the ASM anticyclone) disperse more rapidly and extensively horizontally beyond the ATAL region than particles from other sites. A larger portion of these EA-released particles also reaches the Southern Hemisphere UTLS region.

When aerosols are released below the ATAL (at 11–12 km), vertical motion near the release site significantly influences the number of particles entering the UTLS region. Specifically, aerosols released over South Asia more readily enter the ASM anticyclone and the stratosphere, thus residing longer in the UTLS region.

Given that fact that aerosol mass concentration within the ATAL exhibits a persistent increasing trend over the past decade (Yuan et al., 2019; Bossolasco et al., 2021), the results presented in this study have significant implications for future accurate evaluation of ATAL's climate effects. Estimates of the ATAL's radiative effects in previous studies have based on bulk aerosol properties, without accounting for the critical dependence of radiative efficiency on particle size and atmospheric lifetime (Murphy et al., 2021). The systematic quantification of lifetimes for different sized aerosols in the ATAL in this study provides some essential parameters for more accurate evaluation of the ATAL's climate effects. On the other hand, while the present solar geoengineering proposals related to stratospheric aerosols have large uncertainties in optimal injection location, timing, and frequency (Bednarz et al., 2023; Visioni et al., 2023), the findings in this study offer some detailed, process-based information for the design of stratospheric aerosol injection (SAI) strategies. However, more systematic studies are worthwhile to compare the lifetimes of aerosols injected from the ASM domain with that from other sites to obtain more integrated information for the SAI strategies.

It should be pointed out that our idealized climate model experiments uses chemically inert NCl aerosols as size-fractionated passive tracers with their radiative and chemical effects are disabled in the model. This approach enables us to isolate the dynamical and size-dependent variations on aerosol lifetime and transport properties. However, aerosols in the ATAL have complex composition and various sources with organic aerosols, and sulfate and nitrate aerosols are the dominant components of the real ATAL. Those aerosols involve complex radiative-chemical-dynamical feedbacks in the UTLS, and hence, the lifetime of the ATAL aerosols could also be modulated indirectly by their radiative and chemical effects. This issue is worthy further investigations.

https://doi.org/10.5194/egusphere-2025-6412
Preprint. Discussion started: 26 February 2026

Code and data availability

The codes and model simulations can be downloaded via https://doi.org/10.17605/OSF.IO/UCXEP. The MERRA-2 data are publicly available at https://search.earthdata.nasa.gov/search?q=MERRA2&fst0=Atmosphere (Gelaro et al., 2017). Data analysis and visualization were performed using Matlab R2022a, an openly available version, downloaded from https://ww2.mathworks.cn/downloads/.

Author contributions

The individual contributions of the co-authors, following the CRediT taxonomy, are as follows:

Conceptualization: WT, JL, YD

Methodology: WT, YD, YP

Formal analysis: YD, YL

Investigation (Numerical experiments): YD, YP

Validation: YD, YL, RH

Visualization: YD, HX

Writing – original draft: YD

Writing – review & editing: WT, JL

Supervision: WT

Funding acquisition: WT

Project administration: WT

Competing interests

The authors declare that they have no conflict of interest.

Disclaimer

Copernicus Publications remains neutral with regard to jurisdictional claims made in the text, published maps, institutional affiliations, or any other geographical representation in this paper. While Copernicus Publications makes every effort to include appropriate place names, the final responsibility lies with the authors. Views expressed in the text are those of the authors and do not necessarily reflect the views of the publisher.

https://doi.org/10.5194/egusphere-2025-6412
Preprint. Discussion started: 26 February 2026

Acknowledgements

The CESM project is supported by the National Science Foundation and the Office of Science (BER) of the U.S. Department of Energy. We acknowledge the Global Model Simulation System Platform and the High-Performance Computing Public Service Platform of Lanzhou University.

Financial support

This work is supported by the National Natural Science Foundation of China (42130601, 42505095) and the General Research Project of Hunan Meteorological Administration (CXFZ2026-MSXM03).

Review statement

The review statement will be added by Copernicus Publications listing the handling editor as well as all contributing referees according to their status anonymous or identified.

References

Appel, O., Köllner, F., Dragoneas, A., Hünig, A., Molleker, S., Schlager, H., Mahnke, C., Weigel, R., Port, M., Schulz, C., Drewnick, F., Vogel, B., Stroh, F., and Borrmann, S.: Chemical analysis of the Asian tropopause aerosol layer (ATAL) with emphasis on secondary aerosol particles using aircraft-based in situ aerosol mass spectrometry, Atmos. Chem. Phys., 22, 13607–13630, https://doi.org/10.5194/acp-22-13607-2022, 2022.

Beirle, S., Hörmann, C., Penning de Vries, M., Dörner, S., Kern, C., and Wagner, T.: Estimating the volcanic emission rate and atmospheric lifetime of SO_2 from space: a case study for Kīlauea volcano, Hawai`i, Atmos. Chem. Phys., 14, 8309–8322, https://doi.org/10.5194/acp-14-8309-2014, 2014.

Bednarz, E. M., Visioni, D., Kravitz, B., Jones, A., Haywood, J. M., Richter, J., MacMartin, D. G., and Braesicke, P.: Climate response to off-equatorial stratospheric sulfur injections in three Earth system models – Part 2: Stratospheric and free-tropospheric response, Atmos. Chem. Phys., 23, 687–709, https://doi.org/10.5194/acp-23-687-2023, 2023.

Bian, J.: Recent Advances in the Study of Atmospheric Vertical Structures in Upper Troposphere and Lower Stratosphere, Adv. Earth Sci., 24, 262–271, https://doi.org/10.11867/j.issn.1001-8166.2009.03.0262, 2009 (in Chinese).

Bian, J., Li, D., Bai, Z., Li, Q., Lyu, D., Zhou, X.: Transport of Asian surface pollutants to the global stratosphere from the Tibetan Plateau region during the Asian summer monsoon, Nat. Sci. Rev., 7(3): 516–533, https://www.sciengine.com/doi/10.1093/nsr/nwaa005, 2020.

Binkowski, F. S., and S. J. Roselle: Models-3 Community Multiscale Air Quality (CMAQ) model aerosol component 1. Model description, J. Geophys. Res., 108, 4183, doi:10.1029/2001JD001409, D6, 2003.

https://doi.org/10.5194/egusphere-2025-6412
Preprint. Discussion started: 26 February 2026

Bossolasco, A., Jegou, F., Sellitto, P., Berthet, G., Kloss, C., and Legras, B.: Global modeling studies of composition and decadal trends of the Asian Tropopause Aerosol Layer, Atmos. Chem. Phys., 21, 2745–2764, https://doi.org/10.5194/acp-21-2745-2021, 2021.

Chen, Q. L., Gao, G. L., and Li, Y.: Advances in Studies of Deep Convection over the Tibetan Plateau and Its Effect on Stratospheric–Tropospheric Material Transport, Chin. J. Atmos. Sci., 46, 1198–1208, https://doi.org/10.3878/j.issn.1006-9895.2201.21118, 2022 (in Chinese).

Clemens, J., Vogel, B., Hoffmann, L., Griessbach, S., Thomas, N., Fadnavis, S., Müller, R., Peter, T., and Ploeger, F.: A multi-scenario Lagrangian trajectory analysis to identify source regions of the Asian tropopause aerosol layer on the Indian subcontinent in August 2016, Atmos. Chem. Phys., 24, 763–787, https://doi.org/10.5194/acp-24-763-2024, 2024.

Croft, B., Pierce, J. R., and Martin, R. V.: Interpreting aerosol lifetimes using the GEOS-Chem model and constraints from radionuclide measurements, Atmos. Chem. Phys., 14, 4313–4325, https://doi.org/10.5194/acp-14-4313-2014, 2014.

Cziczo, D.J., Wolf, M.J., Gasparini, B., Münch, S., and Lohmann, U.: Unanticipated Side Effects of Stratospheric Albedo Modification Proposals Due to Aerosol Composition and Phase. Sci. Rep., 9, 18825, https://doi.org/10.1038/s41598-019-53595-3, 2019.

Easter, R. C., S. J. Ghan, Y. Zhang, R. D. Saylor, E. G. Chapman, N. S. Laulainen, H. Abdul-Razzak, L. R. Leung, X. Bian, and R. A. Zaveri: MIRAGE: Model description and evaluation of aerosols and trace gases, J. Geophys. Res., 109, D20210, doi:10.1029/2004JD004571, 2004.

Fairlie, T. D., Liu, H., Vernier, J.-P., Campuzano-Jost, P., Jimenez, J. L., Jo, D. S., Zhang, B., Natarajan, M., Avery, M. A., and Huey, G.: Estimates of regional source contributions to the Asian Tropopause Aerosol Layer using a chemical transport model. J. Geophys. Res.: Atmos., 125, e2019JD031506, https://doi.org/10.1029/2019JD031506, 2020.

Gao, J., Huang, Y., Peng, Y. and Wright, J. S.: Aerosol effects on clear-sky shortwave heating in the Asian monsoon tropopause layer. J. Geophys. Res.: Atmos., 128, e2022JD036956. https://doi.org/10.1029/2022JD036956, 2023.

Garny, H. and Randel, W. J.: Transport pathways from the Asian monsoon anticyclone to the stratosphere, Atmos. Chem. Phys., 16, 2703–2718, https://doi.org/10.5194/acp-16-2703-2016, 2016.

Gelaro, R., McCarty, W., Suárez, M. J., Todling, R., Molod, A., Takacs, L., Randles, C. A., Darmenov, A., Bosilovich, M. G., Reichle, R., Wargan, K., Coy, L., Cullather, R., Draper, C., Akella, S., Buchard, V., Conaty, A., da Silva, A. M., Gu, W., Kim, G., Koster, R., Lucchesi, R., Merkova, D., Nielsen, J. E., Partyka, G., Pawson, S., Putman, W., Rienecker, M., Schubert, S. D., Sienkiewicz, M. and Zhao, B.: The Modern-Era Retrospective Analysis for Research and Applications, Version 2 (MERRA-2), J. Climate, 30(14), 5419-5454, https://doi.org/10.1175/JCLI-D-16-0758.1, 2017.

Johnston, B. and Xie, F.: Characterizing Extratropical Tropopause Bimodality and its Relationship to the Occurrence of Double Tropopauses Using COSMIC GPS Radio Occultation Observations, Remote Sens., 12, 1109, https://doi.org/10.3390/rs12071109, 2020.

https://doi.org/10.5194/egusphere-2025-6412
Preprint. Discussion started: 26 February 2026

Kaneyasu, N., Ohashi, H., Suzuki, F., Okuda, T., and Ikemori, F.: Sulfate Aerosol as a Potential Transport Medium of Radiocesium from the Fukushima Nuclear Accident, Environ. Sci. Technol., 46, 5720–5726, https://doi.org/10.1021/es204667h, 2012.

Kristiansen, N. I., Stohl, A., Olivié, D. J. L., Croft, B., Søvde, O. A., Klein, H., Christoudias, T., Kunkel, D., Leadbetter, S. J., Lee, Y. H., Zhang, K., Tsigaridis, K., Bergman, T., Evangeliou, N., Wang, H., Ma, P.-L., Easter, R. C., Rasch, P. J., Liu, X., Pitari, G., Di Genova, G., Zhao, S. Y., Balkanski, Y., Bauer, S. E., Faluvegi, G. S., Kokkola, H., Martin, R. V., Pierce, J. R., Schulz, M., Shindell, D., Tost, H., and Zhang, H.: Evaluation of observed and modelled aerosol lifetimes using radioactive tracers of opportunity and an ensemble of 19 global models, Atmos. Chem. Phys., 16, 3525–3561, https://doi.org/10.5194/acp-16-3525-2016, 2016.

Lau, W. K. M., Yuan, C., and Li, Z.: Origin, Maintenance and Variability of the Asian Tropopause Aerosol Layer (ATAL): The Roles of Monsoon Dynamics, Sci. Rep., 8, 3960, https://doi.org/10.1038/s41598-018-22267-z, 2018.

Li, C. and Cohen, R. C.: Space-borne estimation of volcanic sulfate aerosol lifetime, J. Geophys. Res. Atmos., 126, e2020JD033883, https://doi.org/10.1029/2020JD033883, 2021.

Li, Q., Fernandez, R. P., Hossaini, R., Iglesias-Suarez, F., Cuevas, C. A., Apel, E. C., Kinnison, D. E., Lamarque, J.-F., and Saiz-Lopez, A.: Reactive halogens increase the global methane lifetime and radiative forcing in the 21st century, Nat. Commun., 13, 2768, https://doi.org/10.1038/s41467-022-30456-8, 2022.

Liu, X., Easter, R. C., Ghan, S. J., Zaveri, R., Rasch, P., Shi, X., Lamarque, J.-F., Gettelman, A., Morrison, H., Vitt, F., Conley, A., Park, S., Neale, R., Hannay, C., Ekman, A. M. L., Hess, P., Mahowald, N., Collins, W., Iacono, M. J., Bretherton, C. S., Flanner, M. G., and Mitchell, D.: Toward a minimal representation of aerosols in climate models: description and evaluation in the Community Atmosphere Model CAM5, Geosci. Model Dev., 5, 709–739, https://doi.org/10.5194/gmd-5-709-2012, 2012.

Ma, S., Zhang, X., Gao, C., Tong, D. Q., Xiu, A., Wu, G., Cao, X., Huang, L., Zhao, H., Zhang, S., Ibarra-Espinosa, S., Wang, X., Li, X., and Dan, M.: Multimodel simulations of a springtime dust storm over northeastern China: implications of an evaluation of four commonly used air quality models (CMAQ v5.2.1, CAMx v6.50, CHIMERE v2017r4, and WRF-Chem v3.9.1), Geosci. Model Dev., 12, 4603–4625, https://doi.org/10.5194/gmd-12-4603-2019, 2019.

Mahnke, C., Weigel, R., Cairo, F., Vernier, J.-P., Afchine, A., Krämer, M., Mitev, V., Matthey, R., Viciani, S., D'Amato, F., Ploeger, F., Deshler, T., and Borrmann, S.: The Asian tropopause aerosol layer within the 2017 monsoon anticyclone: microphysical properties derived from aircraft-borne in situ measurements, Atmos. Chem. Phys., 21, 15259–15282, https://doi.org/10.5194/acp-21-15259-2021, 2021.

Merikanto, J., Napari, I., Vehkamäki, H., Anttila, T., and Kulmala, M.: New parameterization of sulfuric acid-ammonia-water ternary nucleation rates at tropospheric conditions, J. Geophys. Res., 112, eD15207, https://doi.org/10.1029/2006JD007977, 2007.

Mohanakumar, K.: Stratosphere Troposphere Interactions: An Introduction, Springer, Dordrecht, 416 pp., ISBN 978-1-4020-8216-0, https://doi.org/10.1007/978-1-4020-8217-7, 2008.

https://doi.org/10.5194/egusphere-2025-6412
Preprint. Discussion started: 26 February 2026

Murphy, D. M., Froyd, K. D., Bourgeois, I., Brock, C. A., Kupc, A., Peischl, J., Schill, G. P., Thompson, C. R., Williamson, C. J., and Yu, P.: Radiative and chemical implications of the size and composition of aerosol particles in the existing or modified global stratosphere, Atmos. Chem. Phys., 21, 8915–8932, https://doi.org/10.5194/acp-21-8915-2021, 2021.

Ohata, S., Moteki, N., Mori, T., Koike, M., and Kondo, Y.: A key process controlling the wet removal of aerosols: new observational evidence, Sci. Rep., 6, e34113, https://doi.org/10.1038/srep34113, 2016.

Rasch, P. J., Feichter, J., Law, K., Mahowald, N., Penner, J., Benkovitz, C., Genthon, C., Giannakopoulos, C., Kasibhatla, P., Koch, D., Levy, H., Maki, T., Prather, M., Roberts, D. L., Roelofs, G.-J., Stevenson, D., Stockwell, Z., Taguchi, S., Kritz, M., Chipperfield, M., Baldocchi, D., McMurry, P., Barrie, L., Balkanski, Y., Chatfield, R., Kjellstrom, E., Lawrence, M., Lee, H. N., Lelieveld, J., Noone, K. J., Seinfeld, J., Stenchikov, G., Schwartz, S., Walcek, C., and Williamson, D.: A comparison of scavenging and deposition processes in global models: results from the WCRP Cambridge Workshop of 1995, Tellus B, 52, 1025–1056, https://doi.org/10.1034/j.1600-0889.2000.00980.x, 2000.

Rosenlof, K. H.: Changes in water vapor and aerosols and their relation to stratospheric ozone, C. R. Geosci., 350, 376–383, https://doi.org/10.1016/j.crte.2018.06.014, 2018.

Shaddick, G., Thomas, M. L., Mudu, P., Ruggeri, G., and Gumy, S.: Half the world's population are exposed to increasing air pollution, npj Clim. Atmos. Sci., 3, 23, https://doi.org/10.1038/s41612-020-0124-2, 2020.

Sihto, S.-L., Kulmala, M., Kerminen, V.-M., Dal Maso, M., Petäjä, T., Riipinen, I., Korhonen, H., Arnold, F., Janson, R., Boy, M., Laaksonen, A., and Lehtinen, K. E. J.: Atmospheric sulphuric acid and aerosol formation: implications from atmospheric measurements for nucleation and early growth mechanisms, Atmos. Chem. Phys., 6, 4079–4091, https://doi.org/10.5194/acp-6-4079-2006, 2006.

Solomon, S., Stone, K., Yu, P., Murphy, D. M., Kinnison, D., Ravishankara, A. R., and Wang, P.: Chlorine activation and enhanced ozone depletion induced by wildfire aerosol, Nature, 615, 259–264, https://doi.org/10.1038/s41586-022-05683-0, 2023.

Su, H., Jiang, J. H., Liu, X., Penner, J. E., Read, W. G., Massie, S., Schoeberl, M. R., Colarco, P., Livesey, N. J., and Santee, M. L.: Observed Increase of TTL Temperature and Water Vapor in Polluted Clouds over Asia, J. Climate, 24, 2728–2736, https://doi.org/10.1175/2010JCLI3749.1, 2011.

Textor, C., Schulz, M., Guibert, S., Kinne, S., Balkanski, Y., Bauer, S., Berntsen, T., Berglen, T., Boucher, O., Chin, M., Dentener, F., Diehl, T., Easter, R., Feichter, H., Fillmore, D., Ghan, S., Ginoux, P., Gong, S., Grini, A., Hendricks, J., Horowitz, L., Huang, P., Isaksen, I., Iversen, I., Kloster, S., Koch, D., Kirkevåg, A., Kristjansson, J. E., Krol, M., Lauer, A., Lamarque, J. F., Liu, X., Montanaro, V., Myhre, G., Penner, J., Pitari, G., Reddy, S., Seland, Ø., Stier, P., Takemura, T., and Tie, X.: Analysis and quantification of the diversities of aerosol life cycles within AeroCom, Atmos. Chem. Phys., 6, 1777–1813, https://doi.org/10.5194/acp-6-1777-2006, 2006.

Thomason, L. W. and Vernier, J.-P.: Improved SAGE II cloud/aerosol categorization and observations of the Asian tropopause aerosol layer: 1989–2005, Atmos. Chem. Phys., 13, 4605–4616, https://doi.org/10.5194/acp-13-4605-2013, 2013.

https://doi.org/10.5194/egusphere-2025-6412
Preprint. Discussion started: 26 February 2026

Tian, W. S., Huang, J. L., Zhang, J. K., Xie, F., Wang, W. K., and Peng, Y. F.: Role of stratospheric processes in climate change: Advances and challenges, Adv. Atmos. Sci., https://doi.org/10.1007/s00376-023-2341-1, 2023.

Tian, W. S., Bian, J. C., Lu, G. P., Xiao, Z. N., Yin, Z. C., Huang, J. L., Hu, D. Z., Zhou, F., Zhang, C. Y., and Song, X. L.: Variations in the middle and upper atmospheric environment and their impacts on weather and climate disasters: introduction to major project and latest progress, Trans. Atmos. Sci., 48, 8–25, https://doi.org/10.13878/j.cnki.dqkxxb.20241201003, 2025 (in Chinese).

Tobo, Y., Iwasaka, Y., Shi, G.-Y., Kim, Y.-S., Ohashi, T., Tamura, K., and Zhang, D.: Balloon-borne observations of high aerosol concentrations near the summertime tropopause over the Tibetan Plateau, Atmos. Res., 84, 233–241, https://doi.org/10.1016/j.atmosres.2006.08.003, 2007.

Vernier, J.-P., Thomason, L. W., and Kar, J.: CALIPSO detection of an Asian tropopause aerosol layer, Geophys. Res. Lett., 38, L07804, https://doi.org/10.1029/2010GL046614, 2011.

Vernier, J.-P., Fairlie, T. D., Natarajan, M., Wienhold, F. G., Bian, J., Martinsson, B. G., Crumeyrolle, S., Thomason, L. W., and Bedka, K. M.: Increase in upper tropospheric and lower stratospheric aerosol levels and its potential connection with Asian pollution, J. Geophys. Res. Atmos., 120, 1608–1619, https://doi.org/10.1002/2014JD022372, 2015.

Visioni, D., Bednarz, E. M., Lee, W. R., Kravitz, B., Jones, A., Haywood, J. M., and MacMartin, D. G.: Climate response to off-equatorial stratospheric sulfur injections in three Earth system models – Part 1: Experimental protocols and surface changes, Atmos. Chem. Phys., 23, 663–685, https://doi.org/10.5194/acp-23-663-2023, 2023.

Wang, M., Penner, J. E., and Liu, X.: Coupled IMPACT aerosol and NCAR CAM3 model: Evaluation of predicted aerosol number and size distribution, J. Geophys. Res., 114, D06302, https://doi.org/10.1029/2008JD010459, 2009.

Wu, X., Qiao, Q., Chen, B., Wang, X., Hoffmann, L., Griessbach, S., Tian, Y., and Wang, Y.: The influence of the Asian summer monsoon on volcanic aerosol transport in the UTLS region, npj Clim. Atmos. Sci., 6, 11, https://doi.org/10.1038/s41612-023-00339-w, 2023.

Yu, P., Toon, O. B., Neely, R. R., Martinsson, B. G., and Brenninkmeijer, C. A.: Composition and physical properties of the Asian Tropopause Aerosol Layer and the North American Tropospheric Aerosol Layer, Geophys. Res. Lett., 42, 2540–2546, https://doi.org/10.1002/2015GL063181, 2015.

Yu, P., Rosenlof, K. H., Liu, S., Telg, H., Thornberry, T. D., Rollins, A. W., Portmann, R. W., Bai, Z., Ray, E. A., Duan, Y., Pan, L. L., Toon, O. B., Bian, J., and Gao, R. S.: Efficient transport of tropospheric aerosol into the stratosphere via the Asian summer monsoon anticyclone, Proc. Natl. Acad. Sci. U.S.A., 114, 6972–6977, https://doi.org/10.1073/pnas.1701170114, 2017.

Yuan, C., Lau, W. K. M., Li, Z., and Cribb, M.: Relationship between Asian monsoon strength and transport of surface aerosols to the Asian Tropopause Aerosol Layer (ATAL): interannual variability and decadal changes, Atmos. Chem. Phys., 19, 1901–1913, https://doi.org/10.5194/acp-19-1901-2019, 2019.

https://doi.org/10.5194/egusphere-2025-6412
Preprint. Discussion started: 26 February 2026

Zhang, J., Tian, W. S., Long, X., Tian, H. Y., Huang, Q., Xu, P. P., Yang, Q., and Zhang, J. K.: Fact and Simulation of Dust Aerosol Transported to Stratosphere during a Strong Dust Storm in South Xinjiang, Plateau Meteorol., 34, 991–1004, https://doi.org/10.7522/j.issn.1000-0534.2014.00103, 2015. (in Chinese).

Zhang, J., Wu, X., Bian, J., Xia, X., Bai, Z., Liu, Y., Cai, Z., Huo, J., and Lyu, D.: Aerosol variations in the upper troposphere and lower stratosphere over the Tibetan Plateau, Environ. Res. Lett., 15, 094068, https://doi.org/10.1088/1748-9326/ab9b43, 2020.